Fbxl19 recruitment to CpG islands is required for Rnf20-mediated H2B mono-ubiquitination

Bum-Kyu Lee[†], Jiwoon Lee[†], Wenwen Shen, Catherine Rhee, Haewon Chung and Jonghwan Kim[*]

Department of Molecular Biosciences, Institute for Cellular and Molecular Biology, Center for Systems and Synthetic Biology, The University of Texas at Austin, Austin, TX 78712, USA

ABSTRACT

Histone H2B lysine 120 mono-ubiquitination (H2Bub1) catalyzed by Rnf20 has been implicated in normal differentiation of embryonic stem (ES) and adult stem cells. However, it remains unknown how Rnf20 is recruited to its specific target chromosomal loci for the establishment of H2Bub1. Here, we reveal that Fbxl19, a CxxC domain-containing protein, promotes H2Bub1 at the promoters of CpG island-containing genes by interacting with Rnf20. We show that up-regulation of Fbxl19 increases the level of global H2Bub1 in mouse ES cells, while down-regulation of Fbxl19 reduces the level of H2Bub1. Our genome-wide target mapping unveils the preferential occupancy of Fbxl19 on CpG island-containing promoters, and we further discover that chromosomal binding of Fbxl19 is required for H2Bub1 of its targets. Moreover, we reveal that Fbxl19 is critical for proper differentiation of ES cells in collaboration with Rnf20. Altogether, our results demonstrate that Fbxl19 recruitment to CpG islands is required for Rnf20-mediated H2B mono-ubiquitination.

INTRODUCTION

Epigenetic regulations such as DNA methylation and histone modifications are key regulatory mechanisms providing cell-type specific chromatin landscapes as well as gene expression programs. As one of the key regulatory mechanisms governing gene expression programs, DNA methylation is also implicated in proper mammalian development (1,2). DNA methylation occurs primarily at the cytosine of a CpG dinucleotide whose methylation is stably transmitted through the cell cycle progression (1). In mammals, the majority of CpGs are methylated, whereas CpG islands (CGIs) found in CG-enriched regions are largely un-methylated and prevalent at the promoters of ∼50% of well-annotated genes conserved between mouse and human genomes (3–5). A recent study has additionally shown that >10,000 mammalian orphan CGIs (not associated with promoters) are also un-methylated and implicated in development (6). Accordingly, recent studies have suggested the importance of CGIs in global gene expression regulation (7–9).

Multiple prior studies have revealed that proteins containing a CxxC zinc finger domain (CxxC) can specifically recognize non-methylated CGIs so that they can shape the neighboring chromatin landscape by modulating histone modifications with other regulatory factors (8,10–12). Until now, 12 CxxC domain-containing proteins have been reported (13), many of which, such as Dnmt1, Tet1, Tet3 and Kdm2b, play critical roles during embryogenesis and control the pluripotency of embryonic stem (ES) cells through distinct mechanisms (13,14). For instance, while Dnmt1 faithfully propagates DNA methylation during development (1), Tet1 and Tet3 erase DNA methylation at the regulatory elements of pluripotency-related genes by oxidizing methylcytosine to hydroxymethylcytosine (15–17). More recent studies have suggested that the CxxC domain of Kdm2b confers target specificity of Polycomb repressive complex 1 (PRC1) that catalyzes lysine 119 mono-ubiquitination of histone H2A (H2Aub1) onto development-related and lineage-specific marker genes, thereby limiting their transcriptional activation in self-renewing ES cells (10,18). These studies imply that the CxxC domain functions as a key regulatory component determining differential regulatory modes between the genes associated with CpG island-containing (CGI+) promoters and CpG island-depleted (CGI–) promoters by recruiting specific cofactors.

Mono-ubiquitination of H2A and H2B is strongly implicated in transcriptional gene regulation (19,20). Of particular note, differentiation of embryonic and various adult stem cells leads to a global increase in H2Bub1 (21), and the H2Bub1 regulatory pathway is required for successful differentiation of multipotent stem cells and ES cells (22,23).

---

[*]To whom correspondence should be addressed. Tel: +1 512 232 8046; Fax: +1 512 232 8045; Email: jonghwankim@mail.utexas.edu
[†]These authors contributed equally to this work as first authors.

In ES cells, H2Aub1, catalyzed by Ring1b of the PRC1, serves as a repressive mark since PRC1 restrains paused RNA Pol II on development-related genes (24). Conversely, lysine 120 monoubiquitination of histone H2B (H2Bub1) seems to be an activation mark, as genome-wide mapping of H2Bub1 in human HCT116 cells has revealed that the majority of H2Bub1 signatures are located in the gene bodies of actively transcribing genes (19) and associated with histone methylation (25,26). While the depletion of Rnf20, a H2B lysine 120-specific E3 ubiquitin ligase, significantly reduces the level of global H2Bub1 (27), some studies suggested that H2Bub1 might be involved in regulation of only a small number of genes (28). H2Bub1 is also known to promote loosening of chromatin in collaboration with acetylated H4 (29) and is largely located in the exon–intron junction of actively transcribed exons, suggesting a link between H2Bub1 signatures and exon skipping (30). Consistently, H2Bub1 is tightly coupled with the rate of Pol II elongation via PAF1 and pTEFb (31) rather than transcriptional initiation (32,33). Although PAF1 was proposed to recruit Rnf20 onto H2B (31), considering that PAF1 is a RNA Pol II-associated factor, it remains unknown what grants Rnf20 specificity for certain target loci. Moreover, it remains unclear which classes of genes are affected by H2Bub1 during ES cell differentiation, and to what extent their expression is influenced by this epigenetic mark.

Fbxl19 is a member of the Skp1–Cullin–F-box family of E3 ubiquitin ligases. It was initially reported to act in the cytoplasm by regulating the ubiquitination and proteasomal degradation of an interleukin 1 family receptor (34). However, nuclear functions of Fbxl19 have not been reported so far. Notably, Fbxl19 contains the CxxC domain, and is structurally the most closely related to Kdm2b, a CxxC-containing protein recruiting Ring1b responsible for catalyzing H2Aub1, with an exception of the absence of JmjC domain (13). Considering its CxxC domain and known ability to recruit E3 ubiquitin ligase to target proteins in the cytoplasm (13,34), it is conceivable that Fbxl19 may play roles in the nucleus by recognizing non-methylated CGIs with an aid of the CxxC domain, mediating chromatin modifications such as histone ubiquitination.

Here, we report that Fbxl19 specifically binds CGI+ loci and promotes H2Bub1 in collaboration with Rnf20. We first reveal that overexpression (OE) of Fbxl19 increases the global level of H2Bub1, while its depletion reduces H2Bub1, particularly on CGI+ target genes, according to western blot analyses and genome-wide mapping of H2Bub1 signatures in ES cells. Additionally, global mapping of Fbxl19 targets shows that Fbxl19 preferentially occupies the promoters of CGI+ genes. We further provide evidence of Fbxl19-mediated H2Bub1 by showing impaired induction of H2Bub1 during differentiation of Fbxl19-depleted ES cells, as well as physical association between Fbxl19 and Rnf20. In addition, we discovered that some classes of CGI+ genes, such as the PRC-repressed target genes regulated by Kdm2b and Ring1b in self-renewing ES cells, are not associated with H2Bub1 signatures or Fbxl19 occupancy, neither in self-renewing nor in differentiating ES cells. These results imply that Fbxl19 guides Rnf20 in a selective manner to a specific subset of CGI+ genes.

MATERIALS AND METHODS

Cell culture and differentiation

Mouse ES cells (J1) were cultivated in gelatin (0.1%) coated dishes using DMEM (Dulbecco's modified Eagle's medium, Life Technologies) supplemented with 18% fetal bovine serum (FBS, Gemini), 0.1 mM non-essential amino acids (Life Technologies), 1% nucleoside mix (Sigma-Aldrich), 0.1 mM ß-mercaptoethanol (Sigma-Aldrich), 1000 U/ml recombinant leukemia inhibitory factor (LIF, Chemicon), and 50 U/ml penicillin/streptomycin with 2 mM L-glutamine (Life Technologies). Fbxl19 or Rnf20-overexpressing stable cell lines were maintained in the same media described above with the addition of puromycin (Life Technologies) and geneticin (Life Technologies). Differentiation of ES cells was performed by washing cells three times with PBS, and then culturing them in medium without LIF for 4 days. HEK-293T cells were cultured in DMEM supplemented with 10% FBS and 50 U/ml penicillin/streptomycin with 2 mM of L-glutamine (Life Technologies).

Generation of stable cell lines

Fbxl19, Fbxl19 ΔCxxC (Δa.a.1–58), and Rnf20 cDNA were amplified by PCR, and then cloned into the pEF1α-FLBIO vector as previously described (35,36). Each cloned vector was introduced into BirA expressing ES cells (control cells) or Fbxl19 knock-out cells by electroporation. Positive clones were selected after supplementation with puromycin (1 μg/ml) and neomycin (250 μg/ml). Multiple single colonies were picked in 7–10 days, and expression of Fbxl19 or Rnf20 for each clone was monitored by quantitative real time PCR (qRT-PCR) and western blot using streptavidin–HRP (Life Technologies). Fbxl19 KO cell lines were generated using CRISPR–Cas9 system following manufacturer's instructions (Life Technologies). The GeneArtR CRISPR Nuclease Vector System was used to edit the genomic sequence in the Fbxl19 gene locus. The target sequence was GCCTGTGTGCGAACTGAGTG followed by CGG (PAM sequence). J1 ES cells were transfected with the cloned CRISPR–Cas9 nuclease construct using Lipofectamine R2000 (Life Technologies) and incubated for 1 day. Transfected J1 ES cells were enriched by DynabeadsR CD4 Positive Isolation Kit (Life Technologies) and incubated until visible colonies were formed. Individual colonies were picked and successful gene knockout at the target site was verified by sequencing. All primers used for PCR amplification are listed in Supplemental Table S1.

Virus preparation and infections

shRNA clones targeting each of Fbxl19 and Rnf20 were purchased from Sigma-Aldrich (Supplemental Table S1). Lentiviruses expressing a specific shRNA were generated by transfecting 6 μg of pLKO vector containing a specific shRNA, 4 μg of Δ8.9, and 2 μg of VSVG onto 9×10^6 293T cells using the Fugene transfection reagent (Promega). The following day, the medium was replaced with ES cell culture medium (or LIF-medium for differentiation study), and then incubated at 37°C for 24 h. Viral supernatant was collected, filtered with a syringe filter (0.45 μm), and used to

infect ES cells. To knockdown Fbxl19 or Rnf20, 2.5×10^5 J1 ES cells in each well of a 24-well plate were infected with viral particles. Infected cells were cultured overnight, and the medium was replaced by fresh culture medium supplemented with puromycin (1 μg/ml) to select for infected cells. To investigate acute expression changes upon KD, cells were harvested within 48 h after infection. For gene expression analysis, cells were harvested after 4 days of infection.

Gene expression profiling

Gene expression profiling was performed using Affymetrix GeneChip Mouse Genome 430A 2.0 arrays. Total RNAs were extracted using RNeasy plus mini kit (Qiagen). cDNA synthesis, labeling, hybridization, washing, and scanning were conducted at the Microarray Core Facility at Dana-Farber Cancer Institutes (Boston, MA, USA). Expression data were normalized with a robust multi-array average (RMA) normalization method followed by statistical analysis using linear models for microarray data (Limma) package from Bioconductor. After multiple hypotheses testing using the Benjamini–Hochberg (BH) procedure, a *P*-value cut-off of 0.01 was applied to finalize significantly expressed genes.

qRT-PCR

500 ng of total RNA was reverse transcribed into cDNA using qScript (Quanta). The resultant cDNAs were diluted 20-fold with DNase-free water, and then 1 μl of cDNA was used per reaction of qRT-PCR using the SYBR Green PCR kit (Quanta). PCR primer sets for testing gene expression were designed to amplify the junction between two exons using a web-based primer design program, Primer3 (http://bioinfo.ut.ee/primer3/). All primer sequences are listed in Supplemental Table S1. Mean relative expression of tested genes was calculated from biological triplicate.

Co-immunoprecipitation (Co-IP)

Briefly, 2×10^7 cells were harvested and lysed in extraction buffer containing 20 mM HEPES, 300 mM NaCl, 20% glycerol, 0.5% NP40, 1 mM DTT, 1 mM EDTA, and protease inhibitors. Co-IP buffer was made by mixing 1:1 ratio of extraction buffer and dilution buffer (20 mM HEPES, 20% glycerol, 1 mM EDTA and protease inhibitors). After protein quantification, the resultant protein-containing lysate was immunoprecipitated with streptavidin–agarose beads (Invitrogen, #15942050) for 3 h. Then, 10 μl of each lysate sample was saved for an input control. The immunoprecipitated protein–agarose was washed with co-IP buffer four times (10 min each), then one time with TBS buffer (50 mM Tris–HCl and 150 mM NaCl) for 10 min. The pulled-down proteins were eluted by boiling in Laemmli sample buffer (Bio-Rad) for 10 min.

Antibodies

The antibodies used for western blot analyses were: H2Bub1 (Cell Signaling, #5546S; Millipore, 17-650), H2B (Millipore, #07-371), β-Tubulin (Abcam ab6046), Rnf20 (Abcam, ab32629), Rnf40 (Santa Cruz, SC-132079), Cdk9 (Santa Cruz, SC-484), anti-flag (Sigma, #A8592) and streptavidin–HRP (ThermoFisher).

Alkaline phosphatase (AP) staining

Alkaline phosphatase (AP) activity was measured using an alkaline phosphatase detection kit (Millipore, SCR004). Briefly, cells were cultured for 2 days at low to medium density, and then fixed with 4% paraformaldehyde for 1–2 min followed by rinsing with 1× TBS-T buffer (20 mM Tris–HCl, pH 7.4, 150 mM NaCl and 0.05% Tween-20). Stain solution (a mixture of 2:1:1 ratio of Fast Red Violet (FRV) and Naphthol AS-BI phosphate solution, in water) was added to a volume sufficient to cover the cells, and samples were incubated at room temperature in the dark for 15 min. Cell images were taken after rinsing the cells with 1× TBS-T buffer.

Cell growth assay

Proliferation assays were performed using the Cell Counting Kit-8 (Dojindo) according to manufacturer's instructions. Equal numbers of cells seeded in 96-well plates were used to measure growth rate every day for 4 days with a micro-titer plate reader at the absorbance of 490 nm.

Public data sets used

ChIP-sequencing data sets used for the analyses shown in Figure 7A were obtained from Gene Expression Omnibus (GEO) database: GSE34518 (H2Aub1), GSE40860 (Kdm2b), GSE42466 (Ring1B), GSE18776 (Ezh2) and GSE34785 (Pol II Ser2). Gene expression data sets used for the analyses shown in Figure 2A and E were obtained from GEO database under the accession numbers of GSE31271.

ChIP-seq

ChIP and bioChIP reactions were conducted as previously described (35,36). Briefly, cells were cross-linked with 1% formaldehyde for 7 min at room temperature. Formaldehyde was quenched by adding glycine to a final concentration 125 mM for 5 min. Fixed cells were sonicated using a Bioruptor (Diagenode) with a setting of 30 s on and 1 min off for 10 min (three times). Then, sheared chromatin containing an average of 300 bp DNA fragments was used for immunoprecipitation using 50μl of streptavidin-conjugated magnetic beads (Invitrogen). bioChIP of Fbxl19 was conducted using streptavidin-conjugated magnetic beads. ChIP of H2Bub1 was conducted using the antibody obtained from Millipore (5-1312). Enriched ChIP samples were used to generate of sequencing libraries using an NEB ChIP-seq library preparation kit (NEB, E6200L). ChIP-seq libraries were sequenced using Illumina NextSeq 500 or HighSeq 2500 machines.

ChIP-seq data processing

50 or 75 bp reads from ChIP-seq were mapped onto the *Mus musculus* genome assembly (mm9) using a Burrows-Wheeler Aligner (BWA) allowing 2 bp mismatch (37). Numbers of reads information is summarized in Supplemental

Table S2. Mapped reads were applied for peak calling using the model-based analysis for ChIP-seq (MACS) peak caller (38) with a default setting. Mouse genome mm9 repeat-mask file was downloaded from UCSC genome browser. Peaks found in simple redundant regions of the genome were further filtered out. We generated at least duplicates of ChIP-seq data. The sequencing data from this study have been submitted to the NCBI Gene Expression Omnibus (GEO; http://www.ncbi.nlm.nih.gov/geo/) under accession number GSE76570.

TSS profiling

A region of ± 5 kb from the TSS of all well-annotated genes (24,310 genes) was binned (100 bp), and all reads from ChIP-seq were mapped into each bin. Each bin score was calculated by summing up the number of reads assigned into each bin, and then normalized with the total sequencing depth. Average bin scores across genes were plotted to generate averaged read density across the TSSs. For the analysis of CGI-dependent occupancy profiling of ChIP-seq data, we used 13,070 CGI+ and 11,240 CGI- genes obtained by assigning of CGI loci (from USCS genome browser) to neighboring genes. For the heatmap analyses, genes are ranked by total signal intensity of ChIP-seq in a given area ranging upstream 5 kb and downstream 5 kb from the TSS.

Mapping peaks to gene features

To identify target genes of Fbxl19, Fbxl19 binding sites were mapped to the region surrounding 8 kb upstream and 2 kb downstream of the TSS of all RefSeq genes from the Ref-Flat file downloaded from the UCSC genome browser. To assign one binding site to one genomic feature, we used the following hierarchy: promoter > upstream > intron > exon > intergenic regions. A promoter was defined as a region within ± 2 kb from the TSS, and an upstream was defined as a region between 2 and 20 kb upstream from the TSS. Binding sites not assigned to promoter, upstream, intron or exon were considered intergenic target loci.

Overlap analysis

Overlapping binding sites among ChIP-seq data were identified using a moving window across the mouse genome. If the centers of peaks from different ChIP-seq data were discovered within a 500 bp window, we considered them as overlapping peaks.

Correlation analyses

To generate the binding site correlation map, common binding sites of DNA binding proteins were identified by peak calling followed by an overlap analysis. Scores 0 and 1 were assigned to unique and overlapped binding sites of two TFs, respectively. A pairwise Pearson correlation coefficient between the binding sites of two TFs was calculated for each pair of TFs. Clustering analysis and visualization of the data were done by Cluster 3.0 and Java Treeview, respectively (39,40).

RESULTS

H2Bub1 is generally restricted in the gene body of the CGI+ genes

Recent studies have revealed that the level of H2Bub1 is positively associated with gene activity and increased during differentiation of both mouse and human ES cells (19,21). While it is evident that H2Aub1, another histone mono-ubiquitination signature, predominantly exists at the promoter of developmental genes that are repressed in ES cells (20,24,41,42), it is still ambiguous whether the ubiquitination of H2B occurs across the genome globally in an unbiased manner or if it is restricted to certain areas of the genome or certain classes of genes. To answer this question, we mapped the global H2Bub1 signature using chromatin immunoprecipitation (ChIP) coupled with high-throughput sequencing (ChIP-seq) both in self-renewing ES cells and ES cells after differentiation induced by LIF withdrawal (4 days, see Materials and Methods) (Figure 1A). We detected the majority of H2Bub1 signals on the gene body, and confirmed that the H2Bub1 signals fade away toward the 3′ UTR of the target genes as previously reported (Figure 1B and C) (19,30,32). Consistent with previous studies showing the increased level of pan-nuclear H2Bub1 upon differentiation by Western blot (21), our global H2Bub1 signature mapping clearly revealed that differentiation of ES cells boosts the overall levels of H2Bub1 across the gene body of many genes, while lower levels of H2Bub were observed in self-renewing ES cells (Figure 1A and B). Since CGIs are implicated in global gene regulation (7,8) and histone H2Aub1, another mono-ubiquitination mark, is generally restricted to inactive CGI+ genes, we monitored the relationship between global patterns of H2Bub1 signatures and CGIs. Strikingly, H2Bub1 is confined preferentially to CGI+ genes in both self-renewing and differentiated ES cells (Figure 1D and E). However, the levels of H2Bub1 were almost undetectable in the CGI– genes of both cells we tested (Figure 1D and E). ChIP followed by quantitative PCR independently validated the levels of H2Bub1 (Supplemental Figure S1A and S1B). We further monitored the patterns of global H2Bub1 using the data obtained from human MCF7 cells and mouse embryonic fibroblasts (MEFs), confirming the restricted H2Bub1 marks on the CGI+ genes (Supplemental Figure S1C and S1D). These results imply that DNA sequence features, such as CGIs, inherently determine the destination of H2Bub1 across the genomes of various cell types (43,44).

Increased levels of H2Bub1 do not correlate with changes in gene activity upon differentiation of ES cells

Prior studies revealed that H2Bub1 regulates multiple molecular processes including transcriptional elongation (33,45) and transcriptional activation (19,46). Indeed, we confirmed a general positive correlation between the global gene activity and the levels of H2Bub1 within the cell types we tested (Figure 2A). On the other hand, some studies presented that depletion of Rnf20, a H2B-specific mono-ubiquitin ligase, affects the activity of only a small number of genes even with a drastic reduction in H2Bub1 signature (28), and that H2Bub1 is preferentially associated
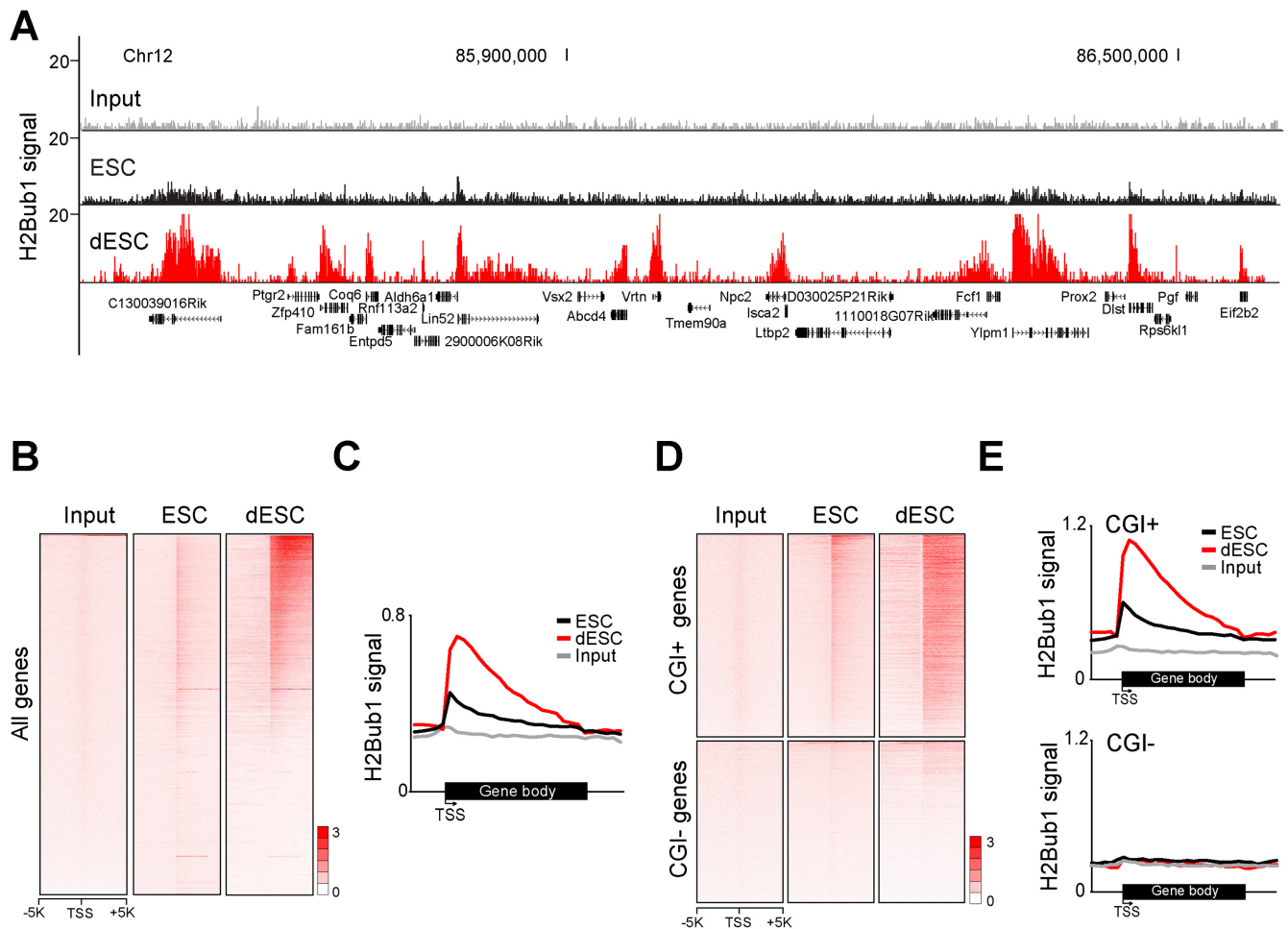
Figure 1. H2B120ub1 is restricted to the gene bodies of the CGI+ genes. (**A**) A snapshot showing signal track image of H2Bub1 signature. (**B**) Heatmaps depicting H2Bub1 signatures within ± 5K (kilobase pair) from transcription start sites (TSSs) of well-annotated genes. (**C**) Average H2Bub1 signals across the gene bodies in both self-renewing (ESC) and differentiated ES cells (dESC). (**D**) Heatmaps presenting H2Bub1 signatures within ±5k from the TSSs of CGI+ and CGI– genes in self-renewing and differentiated ES cells. (**E**) Average H2Bub1 signals across the gene bodies of CGI+ (upper panel) and CGI– (bottom panel) genes in self-renewing and differentiated ES cells.

with the expression of relatively long genes (21). Since we profiled global gene expression and H2Bub1 signatures before and after the differentiation of ES cells, we sought to evaluate the relationship between gene activity and levels of H2Bub1 more carefully. To do this, we first monitored the changes in H2Bub1 levels for CGI+ genes upon differentiation of ES cells (2-fold cutoff), and found that only 115 genes show decreased levels of H2Bub1 (Class I), while more than three thousand genes showed increased levels of H2Bub1 (Class II) (Figure 2B and Supplemental Table S3). This result is consistent with the dramatic increase in H2Bub1 levels upon differentiation of ES cells (Figures 1 and 2A). Interestingly, many of the genes in Class I were previously known pluripotency-associated genes including Klf4, Sox2, Tbx3 and Zfp42 that are down-regulated upon differentiation (Figure 2C–E). This shows that these class I genes experienced a reduction in both gene expression and H2Bub1, which agrees the model that H2Bub1 and expression are positively correlated. In contrast, we found dramatically increased levels of H2Bub1 on the gene body of the Class II genes whose average expression levels were al-

most unchanged rather than increased upon differentiation (Figure 2C–E). The genes in Class II are generally involved in metabolic processes and cell cycle pathways (Figure 2F), and this result surprisingly implies that the increased levels of H2Bub1 are not generally associated with increased gene activity. More surprisingly, our in-depth analyses revealed that some CGI+ genes do not have detectable levels of H2Bub1 in both self-renewing and differentiated cells. These genes are targets of PRC including various lineage marker genes and genes in Hox clusters that are activated upon differentiation of ES cells (Figure 2G). These results indicate that for majority of CGI+ genes, increases in H2Bub1 levels do not positively correlate with the changes in gene expression during ES cell differentiation. The data also reveal that regulation of the PRC targets is largely independent of the H2Bub1 pathway.

Perturbations of Fbxl19 affect the levels of pan-nuclear H2Bub1

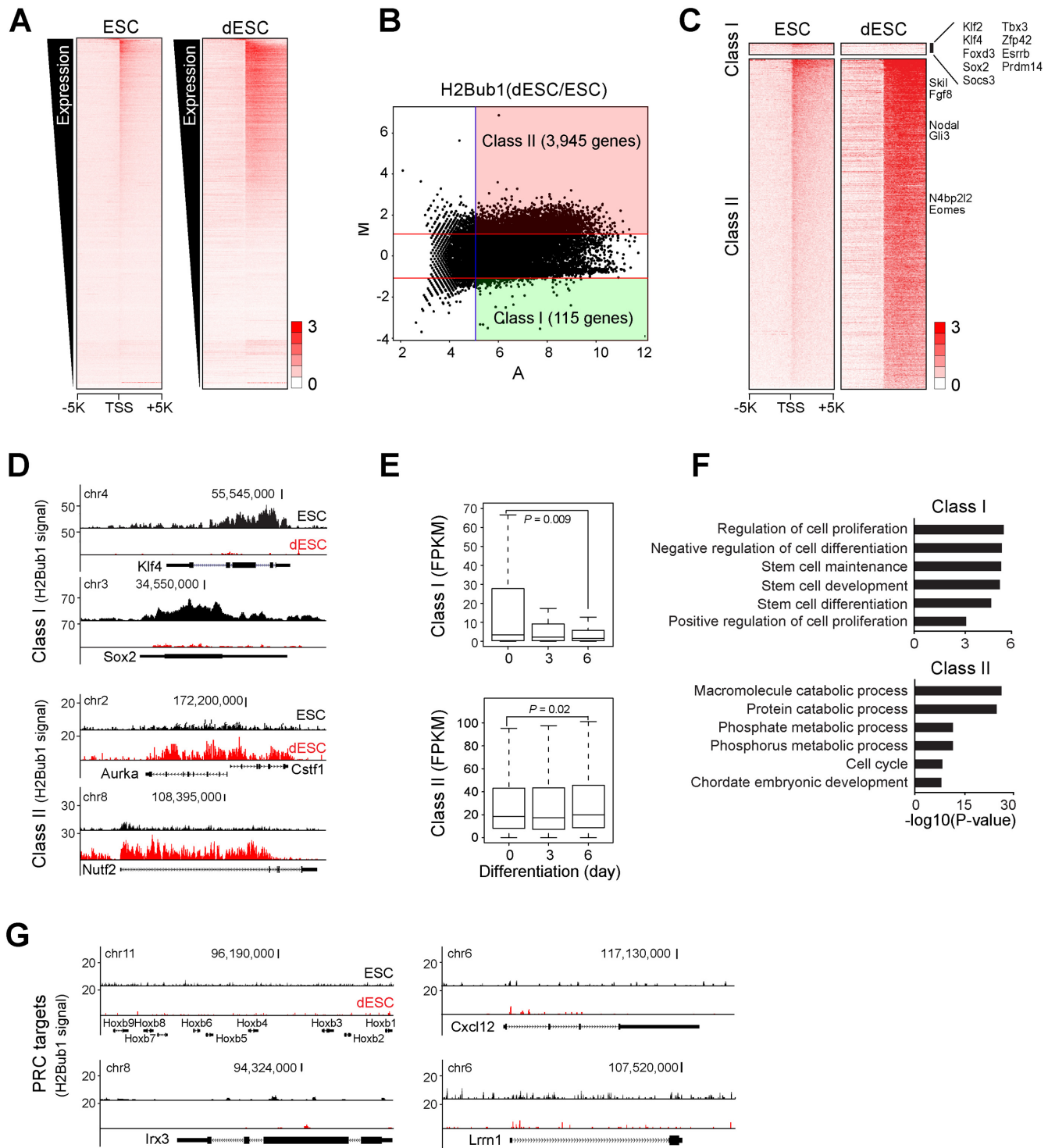In the case of H2A mono-ubiquitination, Kdm2b, a CxxC

Figure 2. H2Bub1 signal is proportional to the gene activity within cells, but the changes in H2Bub1 levels are not correlated with the changes in gene activity during differentiation of ES cells. (**A**) Heatmaps showing H2Bub1 signals within ±5k from the TSSs of well-annotated genes. Expression level of each gene was ranked from high to low, which is shown in black triangle on the left side of each heatmap. (**B**) An MA plot presenting up- and down-regulated H2Bub1 signature of genes during differentiation of ES cells. More than 2-fold cut-off criterion is applied to classify two groups of genes. Class I and Class II genes are associated with decreased and increased levels of H2Bub1 during differentiation of ES cells, respectively. (**C**) Heatmaps showing H2Bub1 signals of each Class of genes in ES cells and differentiated ES cells. H2Bub1 signals in ES cells are ranked from high to low, intensity and corresponding H2Bub1 signals in dESC are shown. Several representative genes in the Class I are shown in black box. (**D**) H2Bub1 signal track images showing representative examples of Class I and Class II genes. (**E**) Boxplots showing gene expression of Class I (upper panel) and Class II (bottom panel) genes during time-course differentiation of ES cells. Gene expression date set was obtained from GEO database under the accession numbers of GSE31271. Wilcox rank sum test was used to calculate *P*-value. (**F**) Bar graphs showing enriched gene ontology (GO) terms of the genes in the Class I (upper panel) and Class II (bottom panel) using David functional annotation tools. (**G**) H2Bub1 signal track images showing representative PRC target genes that do not have significant H2Bub1 signals before and after differentiation of ES cells.

domain-containing protein, recruits PRC1 to CGI+ promoters for generation of H2Aub1 signatures. Since our data showed that H2Bub1 is also restricted to CGI+ genes (Figure 1), we hypothesized that Rnf20 may be also recruited by other CxxC domain-containing proteins to its targets. Among 12 CxxC domain-containing proteins so far reported (13), we were particularly interested in Fbxl19 as a candidate, as Fbxl19 shows structural similarity to Kdm2b (14). Moreover, it has been suggested that Fbxl19 recruits the E3 ubiquitin ligase complex to its target proteins for proteasomal degradation in the cytoplasm (34). To test the roles of Fbxl19 in the H2Bub1 pathway, we first performed shRNA-mediated knockdown (KD) of Fbxl19 in ES cells and monitored the level of global H2Bub1 by western blot analyses. We found that >80% reduction in Fbxl19 significantly curtailed the level of H2Bub1 in ES cells (Figure 3A and B), and testing Fbxl19 KO clones generated by CRISPR-Cas9 genome editing approaches showed a similar reduction in H2Bub1 (Figure 3C and Supplemental Figure S2A). To further test the importance of Fbxl19 in the H2Bub1 pathway, we additionally performed OE of Fbxl19 in ES cells, revealing that OE of Fbxl19 dramatically increased the level of H2Bub1 (Figure 3D and E). These findings clearly indicate that expression of Fbxl19 is positively correlated with levels of the H2Bub1 signature.

Fbxl19 predominantly occupies promoters of CGI+ genes

Until now, nuclear functions of Fbxl19 have not been reported in any cellular context. Since our genome-wide mapping of H2Bub1 signatures has revealed that H2Bub1 is confined within the CGI+ genes (Figure 1), and we found a link between Fbxl19 and H2Bub1 signature, we decided to further investigate the putative roles of Fbxl19 as a nuclear factor in restricting H2Bub1 to CGI+ genes. To do this, we sought to map the chromosomal target loci of Fbxl19 in ES cells. Since we could not find any ChIP-grade or even western-grade native antibody against Fbxl19, we utilized *in vivo* biotinylation approaches as previously described (35). After electroporation of *Fbxl19*-containing plasmids into ES cells, we selected clones expressing a sub-endogenous level of Fbxl19 (OE-low) to mimic native expression levels and clones that expressed a more than 5-fold increased level of Fbxl19 (OE-high) (measured by RT-qPCR). Both categories of clones were then used for further analysis (Supplemental Figure S2B). Using these two clones, we performed bioChIP-seq (7,47) and mapped chromosomal targets of Fbxl19 (Figure 4A). We identified a total of 2213 and 13 669 binding sites of Fbxl19 in Fbxl19 OE-low and OE-high clones, respectively (Supplemental Tables S4 and S5), and these results indicated that Fbxl19 indeed interacts with DNA and has a nuclear function.

As expected, we found that the target occupancy signals of Fbxl19 are much stronger in Fbxl19 OE-high cells (Figure 4A), and the targets of Fbxl19 in OE-low cells are a subset of those in OE-high cells (Supplemental Figure S2C), indicating that an increased level of Fbxl19 in ES cells increases the number of its binding sites across the mouse genome. This result is consistent with the increased level of H2Bub1 upon OE of Fbxl19 tested by Western blot analysis shown in Figure 3E. We found that the majority of Fbxl19

target sites in the OE-high clone are located at the proximal promoters of well-annotated genes while only ~16% of target sites are found at the distal loci from the transcriptional start sites (TSSs) of the annotated genes (Figure 4B). Consistently, proximal promoter binding sites of Fbxl19 showed the strongest occupancy signals across the genome (Supplemental Figure S3A), and further analysis of the target occupancy signals around the CGIs revealed strong enrichment of Fbxl19 at the center of CGI loci (Figure 4C), which is also shown in snapshots of genome track images of representative Fbxl19 binding sites (Figure 4A and D). In-depth inspection of the Fbxl19 signals in CGI+ and CGI– genes revealed that Fbxl19 preferentially occupies the promoters of the CGI+ genes presumably due to the function of the CxxC domain (Figure 4E and F), and strong occupancy signals of Fbxl19 tend to occur at the same loci as H2Bub1 signatures in CGI+ genes (Figure 4G).

Fbxl19 is required for the induction of H2Bub1 during differentiation of ES cells

We next compared the genome-wide occupancy of Fbxl19 with the global H2Bub1 signature in both self-renewing and differentiated ES cells. To visualize the correlation between Fbxl19 occupancy and the level of H2Bub1, we rank-ordered all well-annotated genes based on the occupancy score of Fbxl19 in two groups (CGI+ and CGI– genes), and then plotted their corresponding H2Bub1 signals. As shown in Figures 3E and 5A, the Fbxl19 OE-high clone presented an increased level of H2Bub1 along with a strong occupancy signal of Fbxl19, indicating that Fbxl19 occupancy is generally proportional to H2Bub1 signal, especially for the CGI+ genes. Notably, OE of Fbxl19 in self-renewing ES cells induced the levels of H2Bub1 in CGI+ genes as much as the levels in differentiated cells, meaning that Fbxl19 overexpression alone is sufficient to increase H2Bub1 in CGI+ genes regardless of pluripotency status (Figure 5A and B). Since the levels of H2Bub1 are greatly increased upon differentiation of ES cells (Figure 1), we sought to validate the role of Fbxl19 in the H2Bub1 pathway by examining total H2Bub1 level as well as genome-wide patterns of H2Bub1 signatures using Fbxl19-KD cells under differentiation conditions. From both western blot and ChIP-seq analyses, we confirmed that normal induction of H2Bub1 signatures is significantly impaired during differentiation of Fbxl19-depleted ES cells (Figure 5A–C). Taken together, our data demonstrate that Fbxl19 is required for increase in H2Bub1 observed on CGI+ target genes during ES cell differentiation.

Fbxl19 physically interacts with Rnf20

So far, the Rnf20/40 complex is the only reported histone ubiquitin ligase that catalyzes mono-ubiquitination of H2B lysine 120 in mammalian cells (27,48). Based on our findings that Fbxl19 binds to the promoters of the CGI+ genes and its requirement for mono-ubiquitination of H2B (Figures 4E and 5A), we hypothesized that Fbxl19 may interact with and recruit Rnf20 onto CGI+ targets, similar to the role of Kdm2b in the recruitment of Ring1b of PRC1 onto target developmental genes to generate sub-
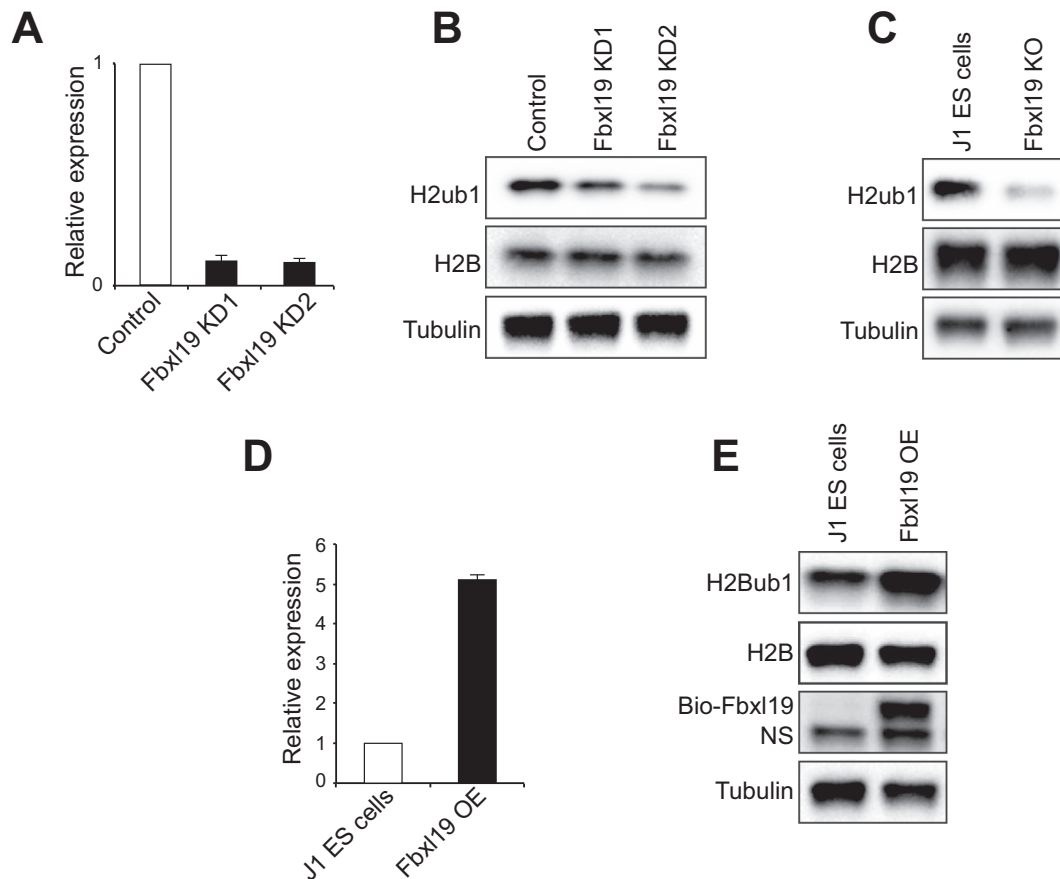
Figure 3. Fbxl19 is implicated in mono-ubiquitination of H2B. (**A**) A bar graph presenting knockdown (KD) efficiency of Fbxl19 measured by qRT-PCR. Error bars indicate standard error of the mean ($n = 3$). (**B** and **C**) Western blots showing decreased levels of H2Bub1 upon KD (B) and KO (C) of Fbxl19. (**D**) A bar graph presenting overexpression (OE) level of Fbxl19 measured by qRT-PCR. Error bar indicates standard error of the mean ($n = 3$). (**E**) Western blots showing induced level of H2Bub1 upon OE of Fbxl19. OE level of Fbxl19 was detected by HRP-conjugated streptavidin. WT indicates wild-type ES cells. NS indicates non-specific band.

sequent H2Aub1 marks (10,18). To test physical associations between Fbxl19 and Rnf20, we performed pull-down of biotin-tagged Fbxl19 using streptavidin beads as previously described (35), and tested its interaction with Rnf20 by Western blot. As shown in Figure 5D, we confirmed that Fbxl19 is physically associated with Rnf20. The result was validated by pull-down of Rnf20 using a native anti-Rnf20 antibody followed by western blot of Fbxl19 using an anti-FLAG antibody (Figure 5E). Since the Rnf20 interactions with Rnf40 and Cdk9 have been previously reported (31), we also tested the association between Fbxl19 and both Rnf40 and Cdk9. We successfully confirmed that Fbxl19 also interacts with these proteins (Figure 5D). To further validate the functional link between Fbxl19 and Rnf20, we conducted KD of Fbxl19 in Rnf20-overexpressing ES cells, and investigated the level of H2Bub1 by western blotting. While slight OE of Rnf20 significantly elevates the level of H2Bub1 (Figure 5F), we found that depletion of Fbxl19 markedly reduced the Rnf20 OE-mediated induction of H2Bub1 (Figure 5F), suggesting that Fbxl19 is required for the Rnf20-mediated H2Bub1. We similarly examined the level of H2Bub1 in Fbxl19 OE-high cells upon KD of Rnf20 and obtained almost complete depletion of H2Bub1 (Fig-

ure 5G). Moreover, bioChIP-seq of Rnf20 showed similar localization patterns of Rnf20 at the Fbxl19 binding sites across the genome (Figure 5H and Supplemental Figure S3B). Taken together, our data suggest that Fbxl19 is required for Rnf20 to catalyze the H2Bub1 signature. The results also imply that the effect of Fbxl19-OE on H2Bub1 shown in Figures 3 and 5 might be attributed to the recruitment of Rnf20 onto the target CGI+ genes. Overall, our results demonstrate that Fbxl19 functions as a critical epigenetic regulator that is indispensable for Rnf20-mediated global H2Bub1 on CGI+ target genes during ES cell differentiation.

CxxC and F-box domains of Fbxl19 are critical for Rnf20-mediated H2Bub1

Fbxl19 has several previously known functional domains, such as CxxC, F-box and LRR domains (13,49). To investigate which domain of Fbxl19 is essential for the Rnf20-mediated H2Bub1, we conducted rescue experiments using an Fbxl19-KO cell line by overexpressing either wild-type Fbxl19 or mutants lacking the CxxC or F-Box domains. OE of wild-type Fbxl19 significantly increased the level of H2Bub1 in Fbxl19 KO cells, confirming the re-
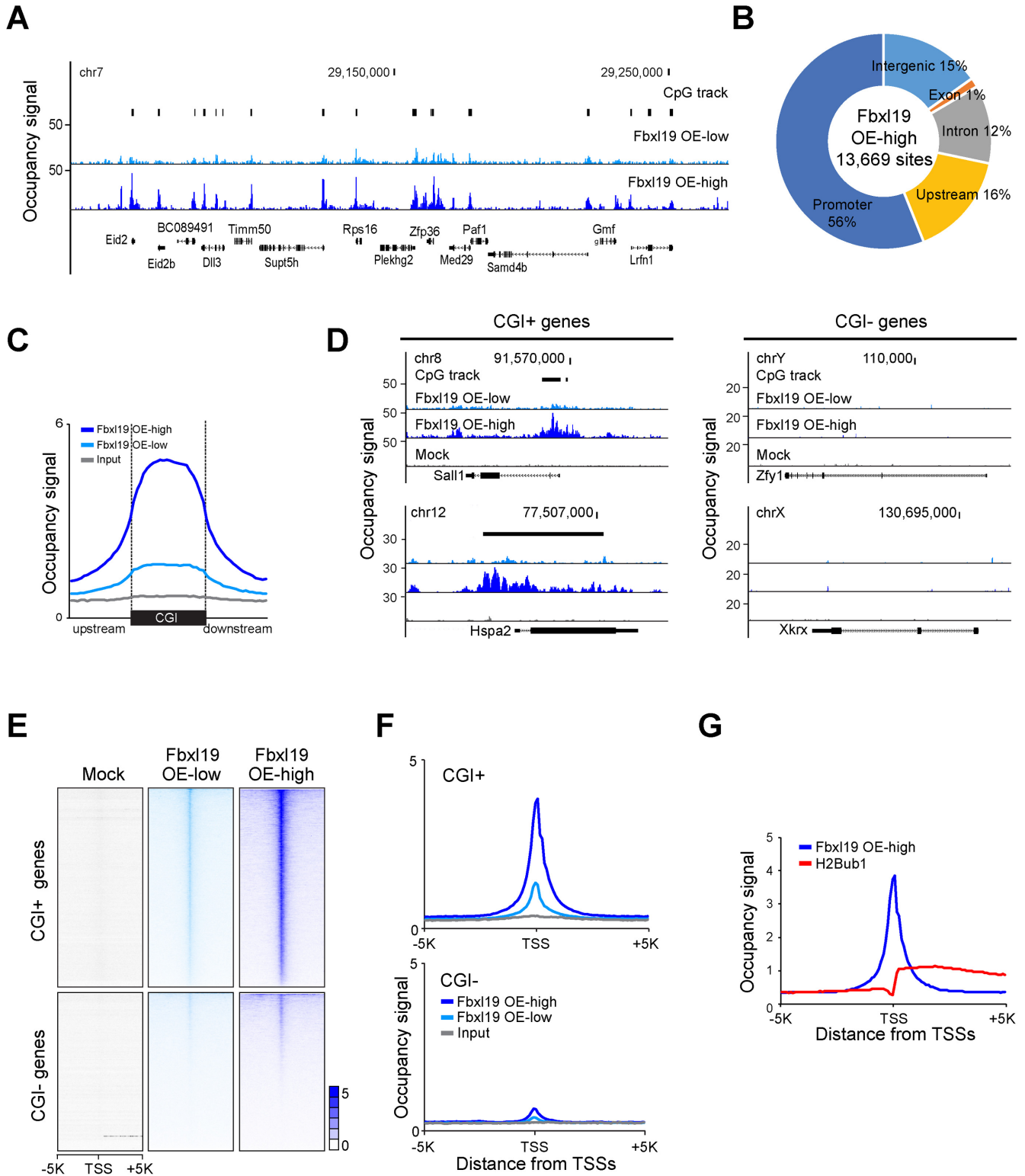
Figure 4. Fbxl19 binds to CGIs and limits H2Bub1 onto CGI+ genes. (**A**) ChIP-seq track images showing Fbxl19 occupancy in Fbxl19 OE-low and OE-high clones. Strong Fbxl19 occupancy signals are observed right at the CGIs. Black bars represent CpG track. (**B**) A pie chart presenting distribution of Fbxl19 binding sites across the mouse genome. Promoters: regions within ±2k from the TSSs; Upstream: regions between 2k and 20k upstream of the TSSs; Intergenic: regions except promoters, upstream, exons, and introns. (**C**) A line plot presenting enriched Fbxl19 occupancy signals at the center of CGI loci. (**D**) ChIP-seq track images showing enriched and depleted occupancy signals of Fbxl19 on CGI+ and CGI– genes, respectively. (**E**) Heatmaps depicting occupancy signals of Fbxl19 within ±5k from the TSSs of CGI+ and CpG– genes in Fbxl19 OE-high and OE-low clones. (**F**) Average occupancy signals of Fbxl19 within ±5k from the TSSs of CGI+ (upper panel) and CGI- (bottom panel) genes in Fbxl19 OE-high and OE-low clones. (**G**) A line graph showing enriched occupancy of Fbxl19 at the TSSs of genes and strong H2Bub1 signatures across the downstream of genes.
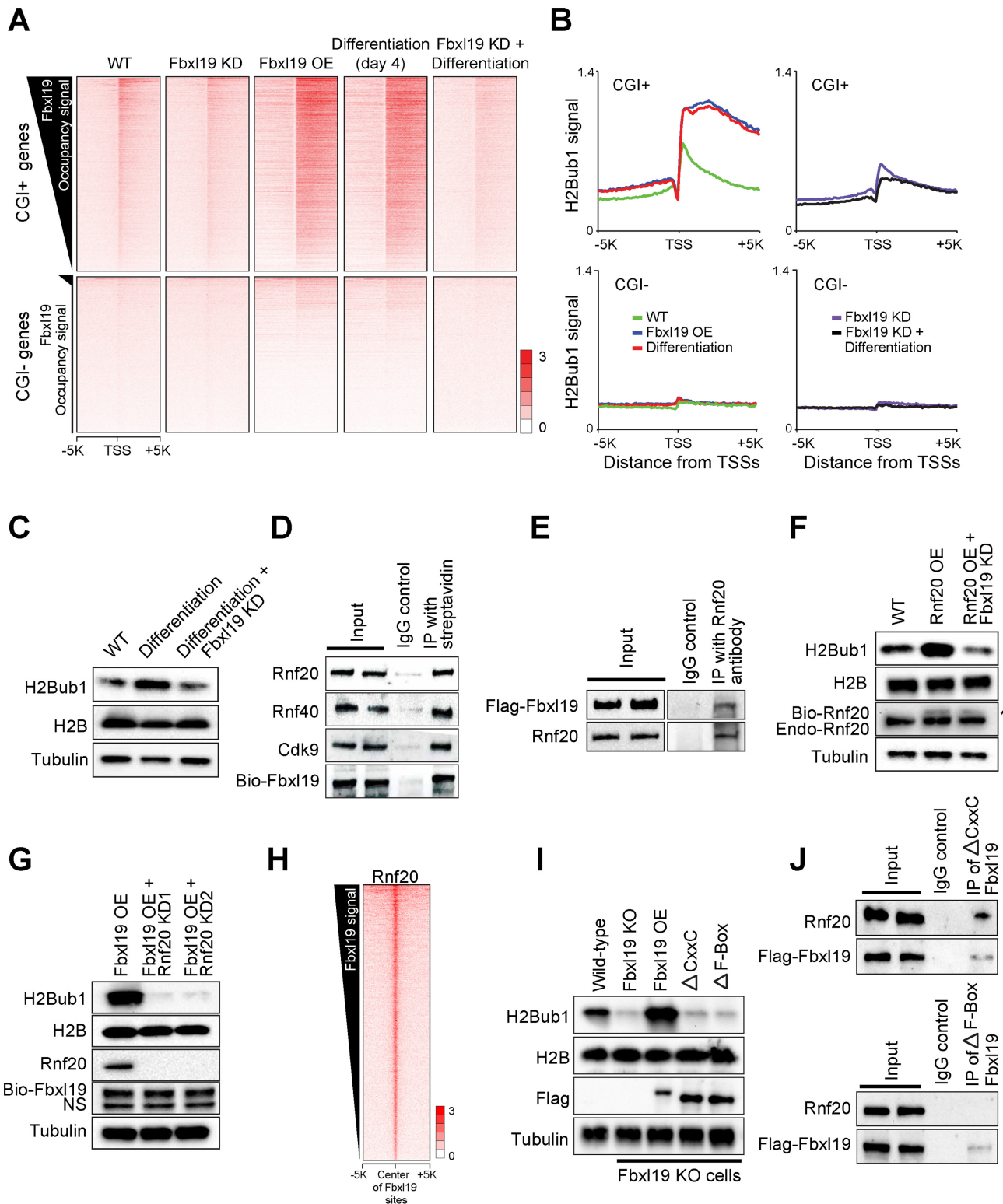
Figure 5. Fbxl19 recruits Rnf20 onto the CGI+ genes. (A-B) Heatmaps (A) and line plots (B) showing H2Bub1 signals detected in WT, Fbxl19-KD, and Fbxl19-OE ES cells, with differentiated Fbxl19-KD cells within ± 5K from TSSs of CGI+ and CGI- genes. (C) Western blots showing impaired induction of H2Bub1 upon differentiation of Fbxl19-KD cells. (D) Immunoprecipitation of Rnf20, Rnf40, and Cdk9 using streptavidin against biotinylated Fbxl19. (E) IP of Fbxl19 using anti-Rnf20 antibody. (F) Western blots presenting levels of H2Bub1 in WT, Rnf20-OE, and Fbxl19-depleted Rnf20-OE cells. Asterisk (*) indicates sub-endogenous level of Rnf20-OE. (G) Western blots showing levels of H2Bub1 upon KD of Rnf20 in Fbxl19-OE cells. (H) A heatmap showing target occupancy patterns of Rnf20 at Fbxl19 target sites. (I) Western blots showing H2Bub1 levels in WT and Fbxl19-KO ES cells as well as Fbxl19-KO cells upon OE of Fbxl19 full-length (Fbxl19-OE), CxxC domain deleted Fbxl19 (ΔCxxC) mutant, and F-box domain deleted Fbxl19 (ΔF-box). WT indicates wild-type J1 ES cells. NS indicates non-specific band. (J) IP of Rnf20 using Fbxl19 deletion mutants.

quirement of Fbxl19 in the induction of H2Bub1 (Figure 5I). On the other hand, we found that OE of CxxC or F-Box domain deletion mutants cannot restore levels of H2Bub1 in Fbxl19-KO cells as compared to OE of full-length Fbxl19 or wild-type cells (Figure 5I), indicating that both domains are necessary for the function of Fbxl19. These results combined with previous knowledge about the roles of the CxxC domain suggest that CxxC domain is required for the guidance of Fbxl19 to CGIs and subsequent H2B mono-ubiquitination. To test the ability of the CxxC domain to recognize the promoters of CGI+ genes, we performed ChIP-qPCR for wild-type and CxxC deletion mutant version of Fbxl19. As shown in Supplemental Figure S3C and S3D, wild-type Fbxl19 strongly occupies tested CGI+ genes while CxxC domain deletion mutant shows dramatically reduced occupancy, suggesting that CxxC domain is critical for binding of Fbxl19 on CGI+ genes. We also performed IP experiments using these mutants to test whether each deleted domain is required for the interaction between Fbxl19 and Rnf20. We found that a deletion of CxxC domain does not affect the interaction of Fbxl19 with Rnf20, while deletion of the F-box abrogates the interaction with Rnf20 (Figure 5J). This suggests that the F-box is essential for the physical interaction between Fbxl19 and Rnf20 in the cell. These results agree with our observation that F-box domain deletion mutant cannot rescue H2Bub1 level as much as wild-type Fbxl19 does in the Fbxl19 KO background (Figure 5I).

Fbxl19 is critical for normal differentiation rather than self-renewal of ES cells

Next, we investigated whether Fbxl19 is crucial for the self-renewal or differentiation of ES cells, given that many CxxC domain-containing proteins play critical roles in ES cells (1,10,15). To investigate the roles of Fbxl19 in ES cells, we not only examined cell morphology and growth rate, but also profiled global gene expression upon perturbation of Fbxl19. We found that the depletion of Fbxl19 by KD or KO does not change typical ES cell morphology, cell growth rate, and alkaline phosphatase activity, while modest reduction of the level of global H2Bub1 was observed (Figures 5A, 6A and B). Consistently, global gene expression profiling analyses with the data obtained from wild-type ES cells, Fbxl19-KD ES cells, and differentiated cells revealed that the expression level of only a few genes are significantly changed upon Fbxl19 depletion, and that the global gene expression patterns are similar between Fbxl19-KD cells and wild-type control cells (Figure 6C and Supplemental Figure S4A). These observations suggest that Fbxl19 is dispensable for the maintenance of self-renewing ES cells.

Conversely, we found that strong induction of Fbxl19 (OE-high cells) causes ES cells to exit from self-renewal and lose their characteristic spheroid morphology (Supplemental Figure S4B). Consistently, Fbxl19 expression gradually increased during differentiation of ES cells (Figure 6D). Global gene expression profile upon OE of Fbxl19 revealed that elevated levels of Fbxl19 promotes induction of many development-related genes evidenced by enriched GO terms of developments (Figure 6E and F), suggesting that Fbxl19 plays a crucial function in pluripotency aspect of ES cells.

To further validate the importance of Fbxl19 in differentiation of ES cells, we monitored ES cell morphology and gene expression on a subset of genes including diverse lineage markers as well as pluripotency-related genes by qRT-PCR upon differentiation of Fbxl19-, Rnf20- or Rnf40-KD cells. Consistent with the previously observed differentiation defects in Rnf20-KD ES cells (21), we found that Fbxl19-depleted ES cells also showed defects in differentiation, evidenced by impaired induction of lineage markers and delayed repression of pluripotency-related genes (Figure 6G). Taken all together, our results suggest that Fbxl19 is a critical factor for normal differentiation of ES cells rather than self-renewal.

Target occupancy patterns of Fbxl19 and Kdm2b segregate H2Bub1 and H2Aub1 signatures on CGI+ targets

Our genome-wide mapping of H2Bub1 showed generally no increase in the levels of H2Bub1 on the bodies of PRC target genes that become active upon differentiation of ES cells. Moreover, these genes had undetectable levels of H2Bub1 in self-renewing ES cells (Figure 2G). These observations suggest that the accessibility of Fbxl19 to CGI+ promoters is also restricted for some class of genes. In turn, the occupancy signals of Fbxl19 on the PRC target genes were also significantly weaker (Supplemental Figure S4C). Since previous studies revealed that Kdm2b is responsible for the generation of H2Aub1 by recruiting Ring1b to the promoters of PRC-repressed target genes that belong to the CGI+ genes (10,18), we sought to compare target occupancy of Fbxl19 and Kdm2b among CGI+ genes. We first ranked the genes based on occupancy ratio of Fbxl19 over Kdm2b, and then plotted the occupancy signals of Fbxl19 and Kdm2b side by side. We additionally plotted corresponding occupancy signals of other factors, such as the elongation form of Pol II (phospho-serine 2) for monitoring active genes, as well as Ring1b and Ezh2 for PRC-repressed target genes along with H2Aub1 and H2Bub1 signatures. As shown by heat maps in Figure 7A, we found that global occupancy patterns of Pol II and Fbxl19 on CGI+ genes are similar, but their occupancy patterns are opposite to those of Kdm2b, Ring1b and Ezh2. Moreover, the patterns of associated H2Bub1 and H2Aub1 tend not to overlap, indicating that these two signatures typically do not occur on the same loci (Figure 7B and C). These results suggest that the recruitment of Rnf20 and Ring1b by Fbxl19 and Kdm2b, respectively, are responsible for differential target gene regulation among CGI+ genes through unique histone modifications.

DISCUSSION

In our study, we have identified Fbxl19 as a key regulator that links Rnf20, an H2B-specific E3 ligase, and CGI elements of the genome for the generation of global H2Bub1 signatures. Perturbations of Fbxl19 directly affected the levels of H2Bub1 in ES cells, and depletion of Fbxl19 severely impaired the induction of H2Bub1 under differentiation conditions. In self-renewing ES cells, levels of H2Bub1 were not very high across the body of active CGI+ genes, although we still detected a positive correlation between gene
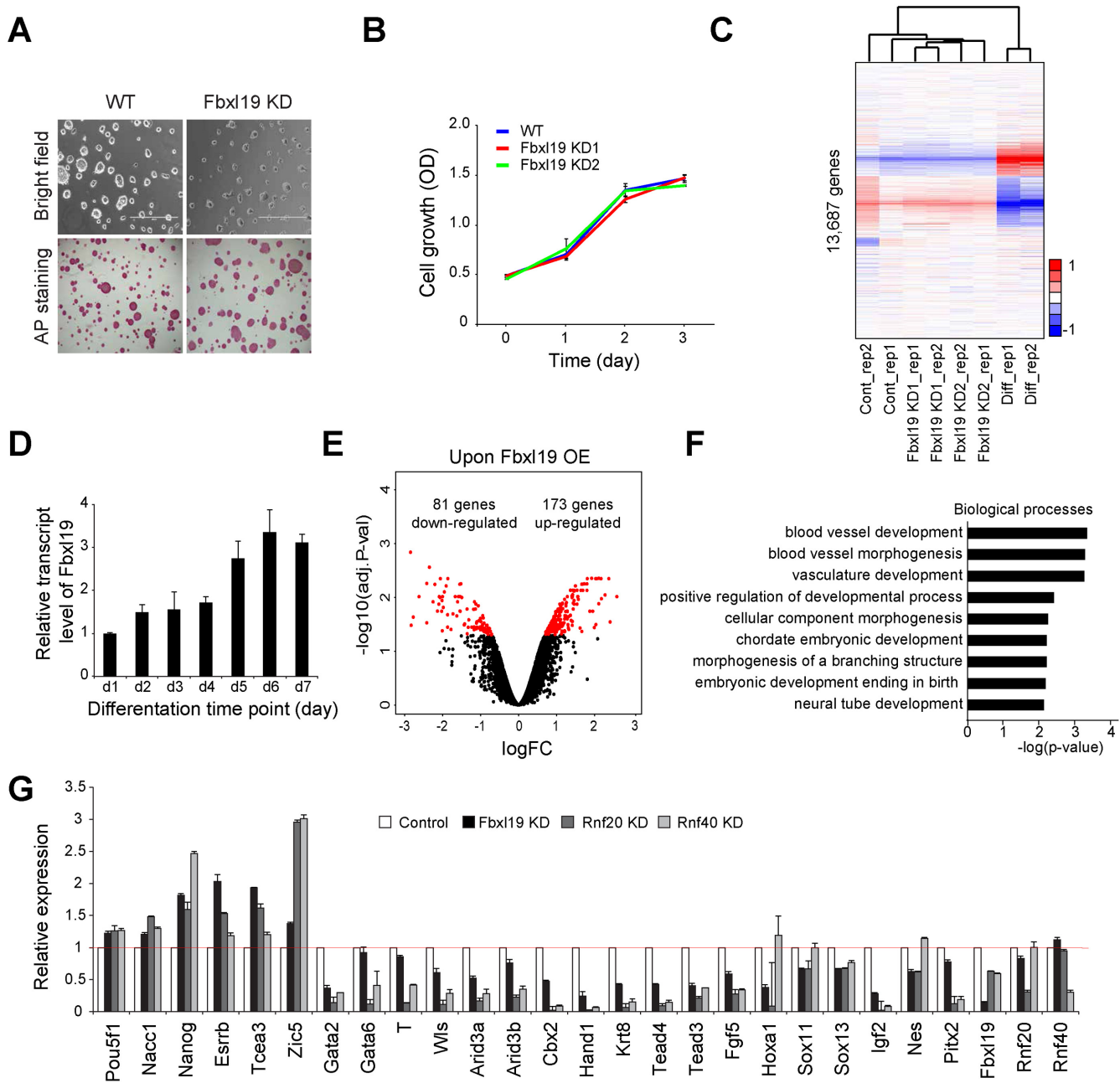
Figure 6. Fbxl19 is indispensible for proper differentiation of ES cells. (**A**) Wild-type and Fbxl19-depleted cells under bright-field and after alkaline phosphatase (AP) staining are shown. (**B**) A line graph demonstrating cell growth of wild-type and Fbxl19-depleted cells. (**C**) A heatmap depicting similar expression patterns between wild-type and Fbxl19-depleted cells, which are separately clustered from differentiated ES cells. (**D**) Relative Fbxl19 transcript levels along with time-course differentiation. Error bars indicate standard error of the mean ($n = 3$). (**E**) A volcano plot showing that many genes are differentially expressed upon OE of Fbxl19. X-axis indicates $\log_2$ fold changes of genes expression between Fbxl19-OE and control cells. Y-axis depicts $-\log_{10} P$-value. (**F**) A bar graph showing the enriched gene ontology (GO) term on the up-regulated genes upon OE of Fbxl19. (**G**) Expression levels of various lineage markers and pluripotency factors during 4-day differentiation of wild-type, Fbxl19-KD, Rnf20-KD and Rnf40-KD ES cells. Error bars indicate standard error of the mean ($n = 4$).

activity and the level of H2Bub1 as previously reported (19,32,46). Considering the drastic increase of H2Bub1 in differentiated ES cells, it is conceivable that this weak level of H2Bub1 in ES cells is attributed to the small subpopulation of spontaneously differentiated cells in serum/LIF culture conditions. Notably, our analyses revealed that alterations in the levels of H2Bub1 do not always correlate with

changes in gene activity during differentiation of ES cells, as evidenced by the increased levels of H2Bub1 in the genes without changes in expression during differentiation. Additionally, some classes of CGI+ genes, such as PRC targets, are not associated with the H2Bub1 signature regardless of gene activity changes upon differentiation. Thus, our results
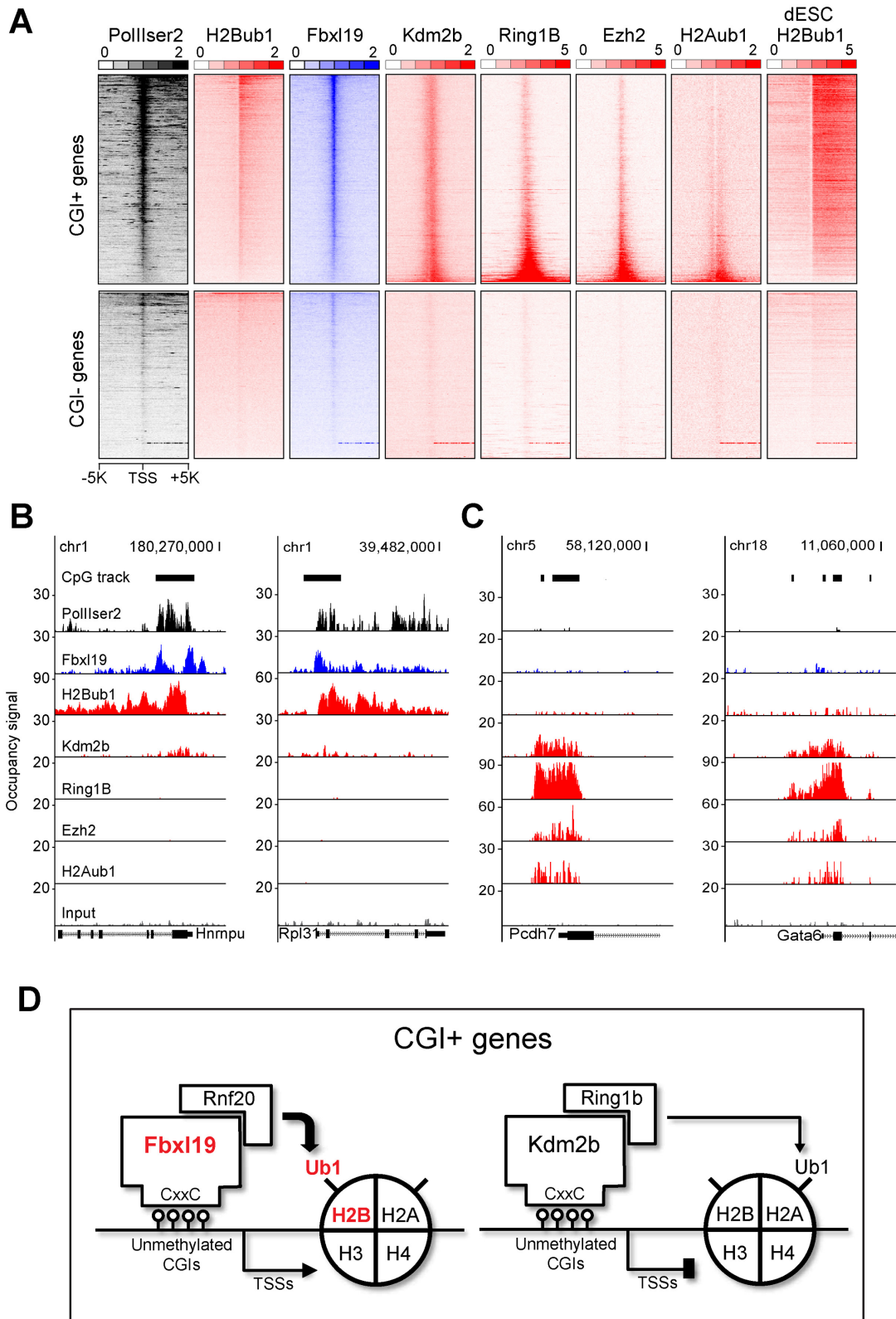
Figure 7. Fbxl19 and Kdm2b have distinct set of targets within CGI+ genes. (**A**) Heatmaps presenting occupancy signals of PolII Ser2, Fbxl19, Kdm2b, Ring1B and Ezh2 in addition to mono-ubiquitination signatures of H2A and H2B in ES cells. H2Bub1 signatures in differentiated cells are also shown (dESC H2Bub1). (**B**) ChIP-seq signal track images showing representative Fbxl19-enriched genes together with H2Bub1 and PolII Ser2 signals. (**C**) ChIP-seq signal track images demonstrating representative Kdm2b-enriched genes with Ring1B, Ezh2 and H2Aub1 signals. (**D**) A model illustrating a mechanism of Fbxl19-mediated mono-ubiquitination of H2B at the CGI+ genes. Fbxl19 recognizes un-methylated CGI+ promoters, and loads Rnf20 for catalyzing mono-ubiquitination of H2B, while Kdm2b recruits Ring1b to CGI+ promoters for H2A mono-ubiquitination.

reveal that the level of H2Bub1 is not the sole indicator of gene activity, but rather one of several such indicators.

Furthermore, we have discovered that Fbxl19 is indispensable for H2Bub1. We showed that KD of Fbxl19 significantly reduces the level of global H2Bub1 while OE increases it, and this increase is particularly strong in CGI+ genes. In addition, our ChIP-seq of Fbxl19 demonstrated that Fbxl19 preferentially occupies the proximal promoter of CGI+ genes, while H2Bub1 largely occurs in the body of CGI+ gene. Its signature gradually diminishes along the 3′ UTR, consistent with the previous studies (19,30,32). This CGI-dependent histone mono-ubiquitination of H2B aided by Fbxl19 is reminiscent of histone mono-ubiquitination on H2A mediated by Kdm2b. Thanks to the CxxC domain of Kdm2b that recruits Ring1b of the PRC1, H2Aub1 is limited at the promoters of the PRC-repressed CGI+ target genes. Since H2Bub1 is also generally restricted to CGI+ genes and Fbxl19 specifically binds onto CGI+ genes, we provide a model explaining how the Fbxl19 and H2Bub1 pathway differs from the Kdm2b and H2Aub1 pathway (Figure 7D). In this model, we propose that Fbxl19 is responsible for the recruitment of Rnf20, an E3 ligase for histone H2B mono-ubiquitination onto CGI+ genes. Interestingly, we observed co-localization pattern between Fbxl19 and Rnf20 mainly at CGI+ promoters, but their occupancy pattern is distinct from the pattern of H2Bub1 signatures. It is noteworthy that previously known histone H2Bub1 specific de-ubiquitination enzyme Usp49 showed similar occupancy pattern at the TSSs of well-annotated genes (50). Although speculative, it is conceivable that mono-ubiquitinated H2B may slide down to the gene body from the promoter area aided by unknown mechanisms.

It is noticeable that H2Bub1 marks are not observed at the genes repressed by PRC even after they become active upon differentiation of ES cells. The results suggest that although both Fbxl19 and Kdm2b harbor the CxxC domain for their interaction with unmethylated CGIs, they do not share common targets. Likewise, as shown in Figure 7A–C, both the occupancy of Fbxl19 and Kdm2b as well as their associated H2Bub1 and H2Aub1 signatures seem to be relatively mutually exclusive of one another. It is known that H2A and H2B form heterodimers to construct nucleosomes (51). Our data suggest that only one of these histone proteins can be dominantly mono-ubiquitinated in the nucleosome. Although we revealed distinct patterns of histone mono-ubiquitination (H2Bub1 versus H2Aub1) and factor occupancy (Fbxl19 versus Kdm2b), underlying mechanisms of how these two proteins selectively discern their target genes remain elusive. It has been recently reported that phosphorylation of H2A is critical for mono-ubiquitination of H2B, suggesting crosstalk between these two histone marks (52). Therefore, it is possible that H2A phosphorylation might prohibit H2A mono-ubiquitination while promoting mono-ubiquitination of H2B. Given that the ratio between Kdm2b and Kdm2a occupancy on CGI+ genes was proposed as a key determinant of the recruitment of Ring1b to the PRC-repressed targets (18), it is also conceivable that Fbxl19 and Kdm2b may compete with each other for occupancy on CGI+ target genes with other associated factors. Recently, Med23 has been proposed as an adaptor linking Rnf20 to its subset of targets (43), and it may be

worthwhile to probe whether there exists a physical interaction between Fbxl19 and Med23.

Multiple CxxC domain-containing proteins play important functions in the physiology of ES cells (1,10,15). From our studies, we found that the Fbxl19-depleted ES cells maintain typical ES cell morphology, cell growth rate, and alkaline phosphatase activity with modest reduction of the level of global H2Bub1. Consistently, KD of Fbxl19 affects expression of only few genes. These results suggest that Fbxl19 is dispensable for the maintenance of self-renewing status of ES cells. Conversely, we revealed that ES cells with strong induction of Fbxl19 (OE-high cells) disrupted normal ES cell morphology, and induced many genes implicated in differentiation. It is noteworthy that the patterns of global H2Bub1 signatures were similar between Fbxl19-OE cells and differentiated ES cells, and Fbxl19-KD cells showed impaired induction of H2Bub1 upon differentiation. Additionally, Fbxl19-KD cells showed a differentiation defect, failing to repress pluripotency markers and induce lineage markers. Thus, our results suggest that Fbxl19 is crucial for normal differentiation of ES cells rather than self-renewal, which is consistent with the previously observed differentiation defects in Rnf20-KD ES cells (21). However, we also observed that PRC targets, which include many lineage marker genes, are not associated with H2Bub1 and Fbxl19. This suggests that impaired differentiation of Fbxl19-KD cells may be in part caused by an indirect outcome of the dysregulation of H2Bub1. Nevertheless, these findings further emphasize the effects of epigenetic marks, specifically mono-ubiquitination, as well as CpG islands on ES cell differentiation, with Fbxl19 and its partner E3 ligase Rnf20 playing key roles.

SUPPLEMENTARY DATA

Supplementary Data are available at NAR Online.

REFERENCES

1. Smith,Z.D. and Meissner,A. (2013) DNA methylation: roles in mammalian development. *Nat. Rev. Genet.*, **14**, 204–220.
2. Walsh,C.P. and Bestor,T.H. (1999) Cytosine methylation and mammalian development. *Genes Dev.*, **13**, 26–34.
3. Deaton,A.M. and Bird,A. (2011) CpG islands and the regulation of transcription. *Genes Dev.*, **25**, 1010–1022.
4. Saxonov,S., Berg,P. and Brutlag,D.L. (2006) A genome-wide analysis of CpG dinucleotides in the human genome distinguishes two distinct classes of promoters. *Proc. Natl. Acad. Sci. U.S.A.*, **103**, 1412–1417.
5. Bird,A. (2002) DNA methylation patterns and epigenetic memory. *Genes Dev.*, **16**, 6–21.

6. Illingworth,R.S., Gruenewald-Schneider,U., Webb,S., Kerr,A.R., James,K.D., Turner,D.J., Smith,C., Harrison,D.J., Andrews,R. and Bird,A.P. (2010) Orphan CpG islands identify numerous conserved promoters in the mammalian genome. *PLoS Genet.*, **6**, e1001134.

7. Beck,S., Lee,B.K., Rhee,C., Song,J., Woo,A.J. and Kim,J. (2014) CpG island-mediated global gene regulatory modes in mouse embryonic stem cells. *Nat. Commun.*, **5**, 5490.

8. Thomson,J.P., Skene,P.J., Selfridge,J., Clouaire,T., Guy,J., Webb,S., Kerr,A.R., Deaton,A., Andrews,R., James,K.D. *et al.* (2010) CpG islands influence chromatin structure via the CpG-binding protein Cfp1. *Nature*, **464**, 1082–1086.

9. Beck,S., Lee,B.K. and Kim,J. (2015) Multi-layered global gene regulation in mouse embryonic stem cells. *Cell. Mol. Life Sci.*, **72**, 199–216.

10. He,J., Shen,L., Wan,M., Taranova,O., Wu,H. and Zhang,Y. (2013) Kdm2b maintains murine embryonic stem cell status by recruiting PRC1 complex to CpG islands of developmental genes. *Nat. Cell Biol.*, **15**, 373–384.

11. Blackledge,N.P., Zhou,J.C., Tolstorukov,M.Y., Farcas,A.M., Park,P.J. and Klose,R.J. (2010) CpG islands recruit a histone H3 lysine 36 demethylase. *Mol. Cell*, **38**, 179–190.

12. Xu,C., Bian,C., Lam,R., Dong,A. and Min,J. (2011) The structural basis for selective binding of non-methylated CpG islands by the CFP1 CXXC domain. *Nat. Commun.*, **2**, 227.

13. Long,H.K., Blackledge,N.P. and Klose,R.J. (2013) ZF-CxxC domain-containing proteins, CpG islands and the chromatin connection. *Biochem. Soc. Trans.*, **41**, 727–740.

14. Frauer,C., Rottach,A., Meilinger,D., Bultmann,S., Fellinger,K., Hasenoder,S., Wang,M., Qin,W., Soding,J., Spada,F. *et al.* (2011) Different binding properties and function of CXXC zinc finger domains in Dnmt1 and Tet1. *PLoS One*, **6**, e16627.

15. Ito,S., D'Alessio,A.C., Taranova,O.V., Hong,K., Sowers,L.C. and Zhang,Y. (2010) Role of Tet proteins in 5mC to 5hmC conversion, ES-cell self-renewal and inner cell mass specification. *Nature*, **466**, 1129–1133.

16. Ficz,G., Branco,M.R., Seisenberger,S., Santos,F., Krueger,F., Hore,T.A., Marques,C.J., Andrews,S. and Reik,W. (2011) Dynamic regulation of 5-hydroxymethylcytosine in mouse ES cells and during differentiation. *Nature*, **473**, 398–402.

17. Wu,H., D'Alessio,A.C., Ito,S., Xia,K., Wang,Z., Cui,K., Zhao,K., Sun,Y.E. and Zhang,Y. (2011) Dual functions of Tet1 in transcriptional regulation in mouse embryonic stem cells. *Nature*, **473**, 389–393.

18. Farcas,A.M., Blackledge,N.P., Sudbery,I., Long,H.K., McGouran,J.F., Rose,N.R., Lee,S., Sims,D., Cerase,A., Sheahan,T.W. *et al.* (2012) KDM2B links the polycomb repressive complex 1 (PRC1) to recognition of CpG islands. *Elife*, **1**, e00205.

19. Minsky,N., Shema,E., Field,Y., Schuster,M., Segal,E. and Oren,M. (2008) Monoubiquitinated H2B is associated with the transcribed region of highly expressed genes in human cells. *Nat. Cell Biol.*, **10**, 483–488.

20. Cao,R., Tsukada,Y. and Zhang,Y. (2005) Role of Bmi-1 and Ring1A in H2A ubiquitylation and Hox gene silencing. *Mol. Cell*, **20**, 845–854.

21. Fuchs,G., Shema,E., Vesterman,R., Kotler,E., Wolchinsky,Z., Wilder,S., Golomb,L., Pribluda,A., Zhang,F., Haj-Yahya,M. *et al.* (2012) RNF20 and USP44 regulate stem cell differentiation by modulating H2B monoubiquitylation. *Mol. Cell*, **46**, 662–673.

22. Karpiuk,O., Najafova,Z., Kramer,F., Hennion,M., Galonska,C., Konig,A., Snaidero,N., Vogel,T., Shchebet,A., Begus-Nahrmann,Y. *et al.* (2012) The histone H2B monoubiquitination regulatory pathway is required for differentiation of multipotent stem cells. *Mol. Cell*, **46**, 705–713.

23. Chen,S., Li,J., Wang,D.L. and Sun,F.L. (2012) Histone H2B lysine 120 monoubiquitination is required for embryonic stem cell differentiation. *Cell Res.*, **22**, 1402–1405.

24. Stock,J.K., Giadrossi,S., Casanova,M., Brookes,E., Vidal,M., Koseki,H., Brockdorff,N., Fisher,A.G. and Pombo,A. (2007) Ring1-mediated ubiquitination of H2A restrains poised RNA polymerase II at bivalent genes in mouse ES cells. *Nat. Cell Biol.*, **9**, 1428–1435.

25. Kim,J., Kim,J.A., McGinty,R.K., Nguyen,U.T., Muir,T.W., Allis,C.D. and Roeder,R.G. (2013) The n-SET domain of Set1 regulates H2B ubiquitylation-dependent H3K4 methylation. *Mol. Cell*, **49**, 1121–1133.

26. Wu,L., Lee,S.Y., Zhou,B., Nguyen,U.T., Muir,T.W., Tan,S. and Dou,Y. (2013) ASH2L regulates ubiquitylation signaling to MLL: trans-regulation of H3 K4 methylation in higher eukaryotes. *Mol. Cell*, **49**, 1108–1120.

27. Kim,J., Hake,S.B. and Roeder,R.G. (2005) The human homolog of yeast BRE1 functions as a transcriptional coactivator through direct activator interactions. *Mol. Cell*, **20**, 759–770.

28. Shema,E., Tirosh,I., Aylon,Y., Huang,J., Ye,C., Moskovits,N., Raver-Shapira,N., Minsky,N., Pirngruber,J., Tarcic,G. *et al.* (2008) The histone H2B-specific ubiquitin ligase RNF20/hBRE1 acts as a putative tumor suppressor through selective regulation of gene expression. *Genes Dev.*, **22**, 2664–2676.

29. Fierz,B., Chatterjee,C., McGinty,R.K., Bar-Dagan,M., Raleigh,D.P. and Muir,T.W. (2011) Histone H2B ubiquitylation disrupts local and higher-order chromatin compaction. *Nat. Chem. Biol.*, **7**, 113–119.

30. Jung,I., Kim,S.K., Kim,M., Han,Y.M., Kim,Y.S., Kim,D. and Lee,D. (2012) H2B monoubiquitylation is a 5′-enriched active transcription mark and correlates with exon-intron structure in human cells. *Genome Res.*, **22**, 1026–1035.

31. Wu,L., Li,L., Zhou,B., Qin,Z. and Dou,Y. (2014) H2B ubiquitylation promotes RNA Pol II processivity via PAF1 and pTEFb. *Mol. Cell*, **54**, 920–931.

32. Fuchs,G., Hollander,D., Voichek,Y., Ast,G. and Oren,M. (2014) Cotranscriptional histone H2B monoubiquitylation is tightly coupled with RNA polymerase II elongation rate. *Genome Res.*, **24**, 1572–1583.

33. Pavri,R., Zhu,B., Li,G., Trojer,P., Mandal,S., Shilatifard,A. and Reinberg,D. (2006) Histone H2B monoubiquitination functions cooperatively with FACT to regulate elongation by RNA polymerase II. *Cell*, **125**, 703–717.

34. Zhao,J., Wei,J., Mialki,R.K., Mallampalli,D.F., Chen,B.B., Coon,T., Zou,C., Mallampalli,R.K. and Zhao,Y. (2012) F-box protein FBXL19-mediated ubiquitination and degradation of the receptor for IL-33 limits pulmonary inflammation. *Nat. Immunol.*, **13**, 651–658.

35. Kim,J., Cantor,A.B., Orkin,S.H. and Wang,J. (2009) Use of in vivo biotinylation to study protein-protein and protein-DNA interactions in mouse embryonic stem cells. *Nat. Protoc.*, **4**, 506–517.

36. Kim,J., Chu,J., Shen,X., Wang,J. and Orkin,S.H. (2008) An extended transcriptional network for pluripotency of embryonic stem cells. *Cell*, **132**, 1049–1061.

37. Li,H. and Durbin,R. (2009) Fast and accurate short read alignment with Burrows-Wheeler transform. *Bioinformatics*, **25**, 1754–1760.

38. Zhang,Y., Liu,T., Meyer,C.A., Eeckhoute,J., Johnson,D.S., Bernstein,B.E., Nusbaum,C., Myers,R.M., Brown,M., Li,W. *et al.* (2008) Model-based analysis of ChIP-Seq (MACS). *Genome Biol.*, **9**, R137.

39. de Hoon,M.J., Imoto,S., Nolan,J. and Miyano,S. (2004) Open source clustering software. *Bioinformatics*, **20**, 1453–1454.

40. Saldanha,A.J. (2004) Java Treeview–extensible visualization of microarray data. *Bioinformatics*, **20**, 3246–3248.

41. Leeb,M. and Wutz,A. (2007) Ring1B is crucial for the regulation of developmental control genes and PRC1 proteins but not X inactivation in embryonic cells. *J. Cell Biol.*, **178**, 219–229.

42. Wang,H., Wang,L., Erdjument-Bromage,H., Vidal,M., Tempst,P., Jones,R.S. and Zhang,Y. (2004) Role of histone H2A ubiquitination in Polycomb silencing. *Nature*, **431**, 873–878.

43. Yao,X., Tang,Z., Fu,X., Yin,J., Liang,Y., Li,C., Li,H., Tian,Q., Roeder,R.G. and Wang,G. (2015) The mediator subunit MED23 couples H2B mono-ubiquitination to transcriptional control and cell fate determination. *EMBO J.*, **34**, 2885–2902.

44. Nagarajan,S., Hossan,T., Alawi,M., Najafova,Z., Indenbirken,D., Bedi,U., Taipaleenmaki,H., Ben-Batalla,I., Scheller,M., Loges,S. *et al.* (2014) Bromodomain protein BRD4 is required for estrogen receptor-dependent enhancer activation and gene transcription. *Cell Rep.*, **8**, 460–469.

45. Xiao,T., Kao,C.F., Krogan,N.J., Sun,Z.W., Greenblatt,J.F., Osley,M.A. and Strahl,B.D. (2005) Histone H2B ubiquitylation is associated with elongating RNA polymerase II. *Mol. Cell. Biol.*, **25**, 637–651.

46. Batta,K., Zhang,Z., Yen,K., Goffman,D.B. and Pugh,B.F. (2011) Genome-wide function of H2B ubiquitylation in promoter and genic regions. *Genes Dev.*, **25**, 2254–2265.

47. Lee,B.K., Shen,W., Lee,J., Rhee,C., Chung,H., Kim,K.Y., Park,I.H. and Kim,J. (2015) Tgif1 counterbalances the activity of core pluripotency factors in mouse embryonic stem cells. *Cell Rep.*, **13**, 52–60.

48. Zhu,B., Zheng,Y., Pham,A.D., Mandal,S.S., Erdjument-Bromage,H., Tempst,P. and Reinberg,D. (2005) Monoubiquitination of human histone H2B: the factors involved and their roles in HOX gene regulation. *Mol. Cell*, **20**, 601–611.

49. Blackledge,N.P., Thomson,J.P. and Skene,P.J. (2013) CpG island chromatin is shaped by recruitment of ZF-CxxC proteins. *Cold Spring Harb. Perspect. Biol.*, **5**, a018648.

50. Zhang,Z., Jones,A., Joo,H.Y., Zhou,D., Cao,Y., Chen,S., Erdjument-Bromage,H., Renfrow,M., He,H., Tempst,P. *et al.* (2013) USP49 deubiquitinates histone H2B and regulates cotranscriptional pre-mRNA splicing. *Genes Dev.*, **27**, 1581–1595.

51. Eickbush,T.H. and Moudrianakis,E.N. (1978) The histone core complex: an octamer assembled by two sets of protein-protein interactions. *Biochemistry*, **17**, 4955–4964.

52. Basnet,H., Su,X.B., Tan,Y., Meisenhelder,J., Merkurjev,D., Ohgi,K.A., Hunter,T., Pillus,L. and Rosenfeld,M.G. (2014) Tyrosine phosphorylation of histone H2A by CK2 regulates transcriptional elongation. *Nature*, **516**, 267–271.